Michigan State University

National Superconducting Cyclotron Laboratory

TIME-SCALES FROM TWO-NEUTRON INTENSITY INTERFEROMETRY FOR THE REACTION $^{40}Ar + ^{165}Ho$ at E/A = 25 MeV

S.J. GAFF, A. GALONSKY, C.K. GELBKE, T. GLASMACHER, M. HUANG, J.J. KRUSE, G.J. KUNDE, R. LEMMON, W.G. LYNCH, M.B. TSANG, J. WANG, P.D. ZECHER, F. DEÁK, Á. HORVÁTH, Á. KISS, Z. SERES, K. IEKI, and Y. IWATA

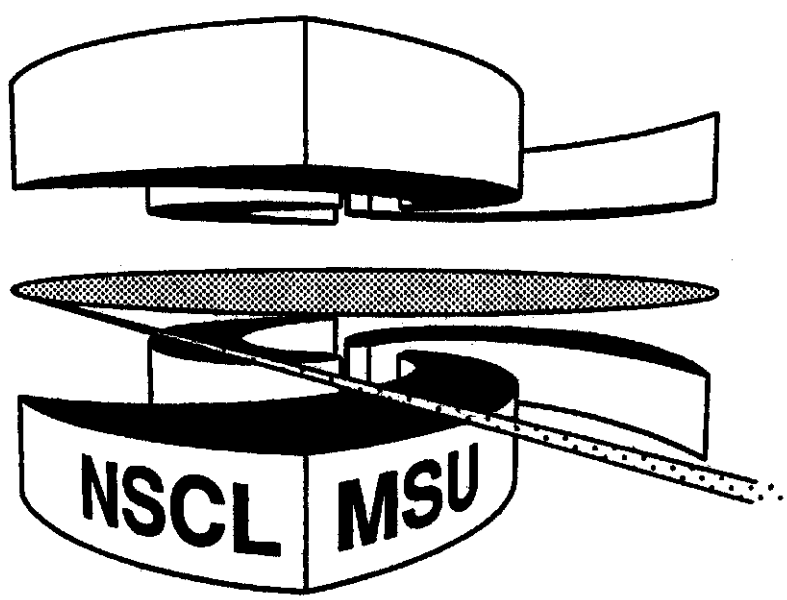

MSUCL-1108

JULY 1998

Time-scales from two-neutron intensity interferometry for the reaction $^{40}Ar + ^{165}Ho$ at E/A = 25 MeV

S.J. Gaff[a], A. Galonsky, C.K. Gelbke, T. Glasmacher, M. Huang[b], J.J. Kruse, G.J. Kunde[c], R. Lemmon[d], W.G. Lynch, M.B. Tsang, J. Wang, P.D. Zecher[e]

National Superconducting Cyclotron Laboratory and Department of Physics and Astronomy

Michigan *State University, East Lansing, Michigan 48824, USA*

F. De&A. Horváth, A. Kiss

Department of Physics, Eötvös University, Budapest, Hungary

Z. Seres

Central Research Institute for Physics, Budapest, Hungary

K. Ieki, Y. Iwata

Rikkyo *University, Tokyo, Japan*

(June 1, 1998)

Abstract

As a test for the time scale of neutron emission, two-neutron intensity interferometry was applied to the reaction $^{40}Ar + ^{165}Ho$ at E/A = 25 MeV. After appropriate corrections for neutron scattering, the correlation function showed a lifetime that was about a factor of two shorter than the lifetime predicted for the statistical decay of an equilibrated nucleus. Preequilibrium emission may explain some of this difference.

PACS number(s): 25.70.Gh

I. INTRODUCTION

In order to describe the forces at work in nuclei, it is important to understand the collective motion of a system of nucleons. One important aspect of describing a nuclear system is the time involved in various processes of the evolution. A clock which can gauge the time for a particular process provides a way to quantify the motion of the nucleons from the nuclear collision to their final state.

Many techniques have been applied to the problem of measuring the time scale in nuclear reactions [1]. Some common techniques are the rate of emission of neutrons, the rate of giant dipole gamma ray (GDR) emission, and crystal blocking. Unfortunately the times measured by these different techniques do not agree. These discrepancies are illustrated by looking at the case of fusion/fission reactions. One analysis using neutron emission rates from a large set of fission data with excitation energies E*=70-210 MeV and comparing them to a "static" statistical model finds fission times of 2-5x10^{-20} s (6000 to 15,000 fm/c) [2]. An alternate analysis, which introduced time-dependent cascade calculations and dynamics into the model, extracted lifetimes from 5x10^{-20} to 10^{-18} s from the same data set (15,000 to 300,000 fm/c) [3]. An experiment measuring GDR gamma rays from a reaction with E*=64 MeV finds a lifetime of 2.9x10^{-19} s (87,000 fm/c) [4]. Another technique, crystal blocking, has recently been modified to be sensitive to fission lifetimes [5]. These results report a lifetime longer than 10^{-19} seconds (30,000 fm/c) for reactions with excitation energies up to 250 MeV. As several of the techniques to measure lifetimes depend on statistical models to interpret the results, it is desirable to have an independent technique to calibrate the models. One such technique which is sensitive to the shorter lifetimes in evaporating systems is two-neutron intensity interferometry.

Two-neutron intensity interferometry is particularly useful in measuring the space-time characteristics of an evaporative system, where the time scale makes charged particle correlations particularly sensitive to distortions from Coulomb re-scattering [6–11]. This technique was applied in the current experiment to the reaction ^{40}Ar + ^{165}Ho at E/A = 25 MeV,

with events selected for centrality by requiring an intermediate mass fragment at a back angle and measuring neutrons at 90°. For this system, where incomplete fusion followed by neutron evaporation is expected in the more central events, the two-neutron intensity interferometry results agree with the predictions of a statistical model within a factor of two, lending credence to the calibration of these models for neutron evaporation time scales.

II. EXPERIMENTAL DETAILS

The current experiment was performed using an ^{40}Ar beam having E/A = 25 MeV produced by the K1200 cyclotron at the National Superconducting Cyclotron Laboratory (NSCL) at Michigan State University. The target was ^{165}Ho with an areal density of 32 mg/cm^2. During the experiment a set of silicon telescopes provided a time reference. Each telescope was made up of two elements, a 75 μm planar Si and a 5 mm Si(Li) detector, and each was located behind a collimator with a diameter of 1.8 cm. In order to select events with small impact parameters which are more likely to form a compound nucleus, a particle with charge $Z \geq 3$ was required in one of these telescopes which were centered at either 30° or 45° [12]. The neutrons were measured in the NSCL Neutron Walls [13]. This array of detectors consists of two walls, each made up of 25 glass cells of liquid scintillator 2 m long, 7.62 cm high, and 6.35 cm deep. Signals from photomultiplier tubes at both ends of each cell were used for pulse shape discrimination and timing. Simulations show that the Neutron Walls are about 10% efficient in measuring 5-40 MeV neutrons when a light threshold of 1 MeV electron equivalent is applied [13]. The time signals, which had about 1 ns resolution, determined both the time of flight and the position along the tube for each hit. The walls were centered around 75° in the laboratory. One was located 4 m from the target, and the second was behind the first and one meter further from the target.

A major difficulty in measuring coincident neutrons is crosstalk: one neutron scattering in two different detectors and leaving a signal in each. In order to eliminate crosstalk the technique suggested in reference [14] was applied. This technique assumes that the

measured neutrons scatter elastically from the protons in the scintillator, which is the most likely mechanism to produce a detectable light signal. This technique cannot distinguish events that result from elastic or inelastic scattering on carbon, but as the neutrons being measured have energies less than 40 MeV most of these events make very little light in the scintillator and so are not detected. Standard scattering kinematics allow calculation of the energy, $E_{n'}$, and scattering angle, θ', of the outgoing neutron, $E_{n'} = E_n - E_p$ and $\cos^2\theta' = E_{n'}/E_n$, from the incident neutron energy, E_n, and the scattered proton's energy, E_p. The neutron energy is calculated from the time-of-flight, and the proton energy is found from the size of the measured light signal. Three criteria are used to compare the measured and calculated values: 1) The difference between the calculated scattering angle, $\cos\theta'$, for the crosstalk neutron and the measured angle between neutron hits, $\cos\theta = \frac{\mathbf{r}_1\cdot(\mathbf{r}_2-\mathbf{r}_1)}{|\mathbf{r}_1||\mathbf{r}_2-\mathbf{r}_1|}$, is restricted to:

$$\Delta C_- < \cos\theta' - \cos\theta < \Delta C_+. \tag{1}$$

2) The difference between the time needed for the scattered neutron to reach the second detector, $t_{n'}$, and the time between hits, $t_2 - t_1$, is restricted to:

$$\Delta T_- < t_{n'} - (t_2 - t_1) < \Delta T_+. \tag{2}$$

3) The difference between the scattered neutron's energy, $E_{n'}$ and the recoil proton's energy for the light measured in the second detector, $E_p(L_2)$, is restricted to:

$$E_{n'} - E_p(L_2) > \Delta E. \tag{3}$$

For a given set of crosstalk parameters – $\Delta C_-, \Delta C_+, \Delta T_-, \Delta T_+$, and ΔE – an event that satisfies all three of these conditions is excluded from the analysis. The values for these parameters were chosen to remove the maximum number of crosstalk events but the minimum number of true coincidences. The effectiveness of this technique was studied by comparison with simulations using GEANT [15] and with a code specifically written to model the Neutron Walls [14]. Both gave similar results and agreed well with the data. Both simulations

include all possible reaction mechanisms for the neutrons with the scintillator and include multiple scattering events. This crosstalk elimination technique is best defined when the hits occur in different walls, so only those events were considered in this analysis. Because the higher-momentum pairs include more crosstalk, it was also necessary to cut on total momentum $|\vec{P}_{tot}| < 250$ MeV/c. In the simulation, the combination of these cuts removes about 97% of the crosstalk and only about 5% of the true coincidence events.

The experimental correlation function is defined in terms of the coincidence neutron yield, $Y_2(\mathbf{p_1}, \mathbf{p_2})$, and the neutron singles yield $Y_1(\mathbf{p})$:

$$\sum Y_2(\mathbf{p_1}, \mathbf{p_2}) = C[1 + R(q)] \sum Y_1(\mathbf{p_1}) Y_1(\mathbf{p_2}). \tag{4}$$

Both sums are over all detector combinations for a given relative momentum, $q = \frac{1}{2}|\mathbf{p_1} - \mathbf{p_2}|$, and both sides are subject to identical cuts and corrections. The singles yield was constructed from events with one and only one neutron because of the ambiguity in how to treat coincidence events that might be crosstalk, although including all multiple hit events did not change the results. Likewise, the coincidence yield contains only the events with exactly two neutrons. The normalization constant, C, was chosen in both the experimental and theoretical correlation functions so that $\langle R(q) \rangle = 0$ for $16 \leq q \leq 40$ MeV/c. The choice of normalization is somewhat arbitrary but was chosen to include the range of q where the data has reasonable error bars and is expected to be flat. The correlation function must be constructed using the singles technique. A mixed event analysis cannot be used because the coincident events include crosstalk. To remove the crosstalk introduces an inefficiency into the data which depends on the momenta of both neutrons which, unlike cuts on the individual momenta, does not cancel within the ratio that forms the correlation function [16]. Fig. 1 shows the experimental correlation function before and after the crosstalk criteria are applied. The crosstalk events produce an artificial peak at $q \sim 10$ MeV/c, not at $q = 0$, because the neutrons are detected at different distances from the target. The correlation function is stable for variations of the parameters, as long as the cut is wide enough to exclude most of the crosstalk.

Because the experiment was performed in a relatively small experimental room, the concrete floor was about one meter away from the bottom of the detectors and the concrete wall was one meter behind the farther detector. This situation introduced a background of in-scattered neutrons from the surrounding material in coincidence with direct neutrons. Some of the background could be removed by making a cut on the light signal compared to the neutron energy reconstructed from the arrival time. Those events where the light deposited exceeded the maximum light response for the reconstructed neutron energy were excluded, as this condition indicates the neutron did not arrive at the detector directly from the target. Also, neutrons with energies less than 5 MeV (those with the longest flight times) were excluded from the analysis. Even after these cuts, about 10% of the singles neutrons come from background, as measured in shadow-bar runs.

On average, the correlation function can be corrected for the remaining background [16]. A corrected correlation function can be defined as

$$1 + R'(q) = \frac{\sum Y_2(\mathbf{p_1}, \mathbf{p_2}) - \alpha \sum Y_1(\mathbf{p_1}) Y_1(\mathbf{p_2}) b(\mathbf{p_1}, \mathbf{p_2})}{\alpha \sum Y_1(\mathbf{p_1}) Y_1(\mathbf{p_2})(1 - b(\mathbf{p_1}, \mathbf{p_2}))}. \tag{5}$$

Here the functions $Y_2(\mathbf{p_1}, \mathbf{p_2})$ and $Y_1(\mathbf{p})$ are the same as in equation (4). The product of the singles yields in the standard correlation function is a distribution reflecting the geometry and efficiency of the detectors without the correlations of the source found in the coincident events. This uncorrelated distribution should be similar to the distribution of scattered events that are added by the background. The function $b(\mathbf{p_1}, \mathbf{p_2})$ is the fraction of times that an event measuring neutrons with momenta $\mathbf{p_1}$ and $\mathbf{p_2}$ would be a background event. This weighting determined from the shadow bar measurements is applied on an event-by-event basis. The correction $b(\mathbf{p_1}, \mathbf{p_2})$ depends on which detectors were hit but is independent of the energies and horizontal positions of the neutrons. The denominator of the corrected correlation function is weighted based on the fraction of events which are not background, $(1 - b(\mathbf{p_1}, \mathbf{p_2}))$. One overall normalization constant, α, is chosen so that $\langle R'(q) \rangle = 0$ for $16 \leq q \leq 40$ MeV/c. The correlation function was corrected for background and the enhancement is about 10%, as shown in Fig. 1.

III. INTERPRETATION OF RESULTS

In order to characterize the results, the correlation function was compared to the results from a simple source emitting neutrons. The neutrons originate from the surface of a sphere with radius r = 7 fm, corresponding to total fusion of the reacting nuclei ($r = 1.2\ A^{1/3}$, A = 205). The emission times are chosen from an exponential distribution, $\exp(-t/\tau)$ described by a lifetime τ. The energy for each neutron is chosen by sampling the efficiency-corrected singles spectrum from the experiment. The energy selected for a neutron is assumed to be completely independent of its emission time. The single-particle phase-space distribution thus produced was filtered using Monte Carlo simulations of the detector response and a correlation function constructed according to the Koonin-Pratt formalism [17,18]. The correlation functions produced before and after filtering are identical at all except the lowest relative momenta [16]. The correlation functions predicted for various lifetimes were compared to the data in Fig. 2, and a lifetime of 700 $\pm$ 200 fm/c was extracted.

As a test of how well a statistical model agrees with the experimental data, a code which implements the statistical formalism of Reference [19] was used. This model predicts the position, time, and energy for particles emitted from an excited source, specified by the initial number of protons and neutrons, the excitation energy, and the energy-level density. These parameters were chosen as follows: First, the mass and charge of the compound nucleus were set equal to the size of the total system, i.e., the effects of preequilibrium emission were assumed to have a small effect on the number of nucleons available to the compound source. Second, since increasing the level density or decreasing the excitation energy changes the shape of the energy spectrum and correlation function in a similar way [16], the level-density parameter was fixed at a = A/10 and the excitation energy was adjusted. A larger level density would produce a steeper energy spectrum, but for this heavy system a = A/10 is already quite large.

The initial excitation energy determines the slope of the energy spectrum. The excitation energy, calculated assuming total fusion, is $E^*/A = 3.93$ MeV. When the predicted energy

spectrum was compared to the efficiency-corrected energy spectrum in the laboratory frame in Fig. 3, the predicted energy spectrum was seen to be too shallow. (The model results were shifted into the laboratory frame by using a center-of-mass velocity of 0.045 c.) To fit the lower-energy part of the measured energy spectrum, the excitation energy was reduced to E*/A = 2.0 MeV. This reduction could be partially explained by assuming a significant amount of incomplete fusion occurred. Previous studies suggest that about 80% of the initial kinetic energy should be transferred to the compound nucleus with the remaining energy carried away by light preequilibrium particles [20,21]. So E*/A = 2.0 MeV was used as a lower limit while 3.93 MeV provided an upper limit for the excitation energy.

When the correlation function predicted by this model is compared to the data in Fig. 2, the value of the calculated correlation function close to $q = 0$ for both limits of the excitation energy is much smaller than the measured correlation function, indicating that the model predicts a slower emission rate; in other words, too long a lifetime for the source. These correlation functions correspond to those calculated for the surface model with r = 7 fm and lifetime parameters of 2000 fm/c when E*/A = 2.0 MeV and 1200 fm/c when E*/A = 3.93 MeV. Possibly, the shorter measured lifetime of 700 ± 200 fm/c can be explained by a contaminant from neutrons emitted before the compound source equilibrated. Even though the neutrons were detected at 90° in the center of mass system where the forward focused preequilibrium neutrons should make a small contribution, some of the neutrons may be coming from this preequilibrium emission. Thus, the measured time may be a combination of a fast neutron component and a slower component of evaporated neutrons.

In order to explore the effects of preequilibrium emission, a fast component was added to the statistical evaporation model [19]. The resulting hybrid model is made up of two independent sources of neutrons, each with its own temperature (energy-spectrum slope parameter). The experimental energy spectrum is fitted by two exponential distributions with temperatures T_c and T_p. The lower temperature, T_c, corresponds to emission from a compound source and is used to choose the excitation energy, while the higher temperature, T_p, sets the slope for the energy spectrum of the preequilibrium emission. To quantify the

fraction preequilibrium/total neutrons, f_p, the energy spectra are compared between 5 and 20 MeV:

$$f_p = \frac{\int_{5MeV}^{20MeV} Ne^{-E/T_p} dE}{\int_{5MeV}^{20MeV} (e^{-E/T_c} + Ne^{-E/T_p}) dE}, \tag{6}$$

where N is the weighting for the preequilibrium component determined by fitting the experimental energy spectrum. The correlation functions were constructed from neutrons sampled from these two distributions with appropriate weights. The energy, emission time and initial position of the compound-source neutrons were determined by the evaporation model. The preequilibrium source has neutron energies sampled from an exponential distribution with temperature, T_p. The emission points were sampled from the surface of a sphere with r = 7 fm, and the emission time was chosen, for simplicity, as $\tau_p = 0$.

Allowing for some systematic uncertainties, the decomposition of the energy spectrum into two components is not unique. By adjusting T_c and T_p, a range of weighting factors can be chosen, all with similar χ^2 values. One possibility, for f_p=18%, is shown in Fig. 3. Correlation functions were constructed for various weights with the appropriate temperatures. Assuming that the evaporation model is accurately determining the emission time of the compound source and the preequilibrium emission is instantaneous ($\tau_p = 0$), the correlation functions can be reproduced by assuming that 25% of the neutrons come from preequilibrium emission. Fig. 4 illustrates this result. If the preequilibrium emission time is not zero, a larger fraction of preequilibrium would be necessary to reproduce the experimental correlation function.

To estimate what would be a reasonable fraction of preequilibrium neutrons to expect in the ^{40}Ar + ^{165}Ho reaction, a model must be applied. Calculations based on the Boltzman-Uehling-Uhlenbeck (BUU) equations [22–24] were used to estimate the shape of the energy spectrum for the preequilibrium component and thus, by comparison to the experimental energy spectrum, determine the fraction of preequilibrium neutrons. The model was run for 200 fm/c, but the slope of the energy spectrum is fairly constant over this time, so the choice of the time cutoff is not important. The BUU results, with a geometrical average over impact

parameters b = 1 - 5 fm, have an energy spectrum with a slope parameter corresponding to a temperature T_p = 12 MeV. This temperature and the experimental energy spectrum require f_p = 18%. The correlation function constructed for this combination of sources, with $\tau_p = 0$, is also shown in Fig. 4. Introduction of a lifetime to the preequilibrium component reduces the correlation function. For example, the particle emission times in the BUU calculations correspond to a lifetime of τ_p = 50 fm/c. Using this lifetime for the preequilibrium component reduces the correlation function at $q = 5$ from $1 + R(q) = 1.26$ to $1 + R(q) = 1.23$.

The value of the correlation function with the preequilibrium fraction predicted by BUU is still smaller than the data close to $q = 0$. In order to assess the difference between the time predicted by the evaporation model with 18% preequilibrium neutrons and the experimental result, the emission time in the model, t_e, was scaled for each event. The new time, $t = st_e$, is used for the compound-source component in the two-component model. This calculation retains the correlation (within a factor s) between the emission time and particle energy as predicted by the statistical model. For the preequilibrium component the slope is taken as T_p = 12 MeV with f_p = 18%, and the emission time is taken as $\tau_p = 0$. Fig. 5 shows that using a scaling factor $s = 0.4$ brings the results into the best agreement with the data.

IV. CONCLUSION

In summary, the measured total correlation function can be described by a source of radius, r = 7 fm and an exponential lifetime of 700 ± 200 fm/c, while a statistical evaporation model would be consistent with a surface-model parameterization of 2000 fm/c with r = 7 fm. This discrepancy can be reduced by including preequilibrium emission in the calculations. The addition of 25% preequilibrium with $\tau_p = 0$ can enhance the correlation function from the evaporation model so that it fits the data. Using the Boltzman-Uehling-Uhlenbeck equations to predict the preequilibrium temperature implies that 18% of the neutrons come from preequilibrium, but this fraction of preequilibrium neutrons produces a correlation

function which is too small. In order to use $f_p = 18\%$ and reproduce the experimental correlation function the emission times for the evaporation neutrons of the hybrid model are scaled by a factor of 0.4.

The present investigation suggests that neutron evaporation clocks are accurate within about a factor of two. Neutron emission may be faster than that predicted by the statistical model used, within this factor of two. The accuracy of our time-scale calibration is limited, however, by uncertainties in contributions from preequilibrium emission. Neither the spectral shape nor the exact time scale is known for the preequilibrium emission in a model independent fashion. An improved calibration of neutron clocks could be possible with measurements at lower beam energies where preequilibrium emission can be safely neglected.

ACKNOWLEDGMENTS

The authors gratefully acknowledge W. Bauer for providing the BUU calculations and S. Pratt for valuable discussions. This work was supported by the National Science Foundation under Grant No. PHY-95-28844, by the Hungarian Academy of Sciences under Grant OTKA 2181 and by the Ministry of Education, Science, Sports and Culture of Japan under Grant Nos. 07640421, 08640392, and 08044095.

REFERENCES

[a] Present address: Triangle Universities Nuclear Laboratory, Duke University, Box 90308, Durham, N.C., USA 27708-0308.

[b] Present address: Sinanet, 202245 Stevens Creek Blvd., Cupertino, CA 95014.

[c] Present address: Yale University, Physics Department, Sloane Physics Laboratory, P.O. Box 208120, New Haven, CT 06520-8120.

[d] Present address: CCLRC Daresbury Laboratory, Daresbury, Cheshire WA44AD, United Kingdom.

[e] Present address: Deloitte & Touche Consulting Group, Two World Financial Center, New York, NY 10281-1420.

[1] D. Hilscher and H. Rossner, Ann. Phys. Fr. **17**, 471 (1992).

[2] D.J. Hinde, D. Hilscher, H. Rossner, B. Gebauer, M. Lehmann, and M. Wilpert, Phys. Rev. C **45**, 1229 (1992).

[3] K. Siwek-Wilczynska, J. Wilczynski, R.H. Siemssen and H.W. Wilschut, Phys. Rev. C **51** 2054 (1995).

[4] R. Butsch, D.J. Hofman, C.P. Montoya, P. Paul, and M. Thoennessen, Phys. Rev. C **44**, 1515 (1991).

[5] M. Morjean, M. Chevallier, C. Cohen, D. Dauvergne, J. Dural, J. Galin, F. Goldenbaum, D. Jacquet, R. Kirsch, E. Lienard, B. Lott, A. Peghaire, Y. Perier, J.C. Poizat, G. Prevot, J. Remillieux, D. Schmaus, M. Toulemonde, Preprint Ganil P97 21 (1997).

[6] W.G. Gong, Y.D. Kim and C.K. Gelbke, Phys. Rev. C **45**, 863 (1992).

[7] P.A. DeYoung, M.S. Cordon, Xiu qin Lu, R.L. McGrath, J. M. Alexander, D.M. de Castro Rizzo, and L.C. Vaz, Phys. Rev. C **39**, 128 (1989).

[8] B. Jakobsson, B. Norén, A. Oskarsson, M. Westenius, M. Cronqvist, S. Mattson, M. Rydehell, Ö. Skeppstedt, J.C. Gondrand, B. Khelfaoui, S. Kox, F. Merchez, C. Perrin, D. Rebreyend, L. Westerberg and S. Pratt, Phys. Rev. C **44**, R1238 (1991).

[9] R. Ghetti, L. Carlén, M. Cronqvist, B. Jakobsson, F. Merchez, B. Norén, D. Rebreyend, M. Rydehell, Ö. Skeppstedt and L. Westerberg, NIM **335**, 156 (1993).

[10] N. Colonna, D.R. Bowman, L. Celano, G. D'Erasmo, E.M. Fiore, A. Pantaleo, V. Paticchio, G. Tagiente, and S. Pratt, Phys. Rev. Lett. **75**, 4190 (1995).

[11] D.A. DeYoung, R. Bennink, T. Butler, W. Chung, C. Dykstra, G. Gilfoyle, J. Hinnefeld, M. Kaplan, J.J. Kolata, R.A. Kryger, J. Kugi, C. Mader, M. Nimchek, P. Santi, A. Snyder, Nuc Phys. A **597**, 127 (1996).

[12] Y.D. Kim, M.B. Tsang, C.K. Gelbke, W.G. Lynch, N. Carlin, Z. Chen, R. Fox, W.G. Gong, T. Murakami, T.K. Nayak, R.M. Ronningen, H.M. Xu, F. Zhu, W. Bauer, L.G. Sobotka, D. Stracener, D. G. Sarantites, Z. Majka, And V. Abnante, H. Griffin, Phys. Rev. Lett. **63**, 494 (1989).

[13] P.D. Zecher, A. Galonsky, J.J. Kruse, S.J. Gaff, J. Ottarson, J. Wang, F. Deák, Á. Horváth, Á. Kiss, Z. Seres, K. Ieki, Y. Iwata, and H. Schelin, NIM **401**, 329 (1997).

[14] J. Wang, A. Galonsky, J.J. Kruse, P.D. Zecher, F. Deák, Á. Horváth, Á. Kiss, Z. Seres, K. Ieki, and Y. Iwata, NIM **397**, 380 (1997).

[15] GEANT Manual, CERN Program Library Long Writeup W5013. Found at WWW site: http://wwwinfo.cern.ch/asdoc/geant_html3/geantall.html.

[16] S.J. Gaff, Ph.D. thesis, Michigan State University, 1997.

[17] S.E. Koonin, Phys. Lett. **70B**, 43 (1977).

[18] S. Pratt and M.B. Tsang, Phys. Rev. C **36**, 2390 (1987).

[19] W.A. Friedman, W.G. Lynch, Phys. Rev. C **28**, 16 (1983).

[20] V.E. Viola, Jr., B.B. Black, K.L. Wolf, T.C. Awes, C.K. Gelbke, H. Breuer, Phys. Rev. C **26**, 178 (1982).

[21] J.B. Natowitz, S. Leray, R. Lucas, C. Ngö, E. Tomasi, and C. Volant, Z. Phys. A **325**, 467 (1986).

[22] W. Bauer, Nucl. Phys. A **471**, 604 (1987).

[23] B.A. Li and W. Bauer, Phys. Rev. C **44**, 450 (1991).

[24] W. Bauer, C.K. Gelbke, and S. Pratt, Annu. Rev. Nucl. Part. Sci. **42**, 77 (1992).

FIGURES

FIG. 1. The correlation function before any corrections compared to the results after corrections were made. All three cases include only neutron pairs with energies greater than 5 MeV and total momentum less than 250 MeV/c. The triangles represent the correlation function with no corrections. The open circles show the correlation function after the crosstalk elimination. The filled circles are the final results with crosstalk elimination and the background corrections.

FIG. 2. Comparison of the experimental correlation function to model calculations. The points show the data after the crosstalk elimination and background corrections. The solid lines are calculated from a surface emission model with a source radius r = 7 fm. The dashed lines are the results from the evaporation model with the excitation energies indicated. The model results are filtered to take into account cuts on neutron energy and total momentum applied to the data and the finite solid angle covered by the detectors. The surface model includes detector response and crosstalk elimination.

FIG. 3. The experimental energy spectrum compared to fits used in model calculations. The data have been corrected for efficiency by using the results of the GEANT simulation. The evaporation-model spectra (solid lines) show the results for both the total excitation energy available to the system and the reduced excitation energy that fits the lower energy part of the experimental spectrum. A two-component fit made of a preequilibrium component and a compound-source component, which are shown separately, are combined with f_p=18% to fit the total spectrum (dashed lines). All the spectra are normalized to the data at E = 6 MeV.

FIG. 4. The experimental correlation function compared to a two-component model. The compound source component of the model has energy, position and emission time as predicted by the evaporation model, while the preequilibrium component uses surface emission with an exponential energy distribution and τ_p=0. The weighting, f_p, gives the fraction of preequilibrium neutrons for energies between 5 and 20 MeV, as defined in the text. For each value of f_p, the experimental energy spectrum was used to constrain the slope of the energy spectra for the preequilibrium component and the excitation energy for the compound-source component.

FIG. 5. The experimental correlation function compared to a two-component modified evaporation calculation. Here the data are compared to the evaporation model with E*/A=2.0 MeV. The emission time from the model is scaled by a factor, s. The simulation includes a contribution from preequilibrium neutrons with f_p=18%.

Figure 1

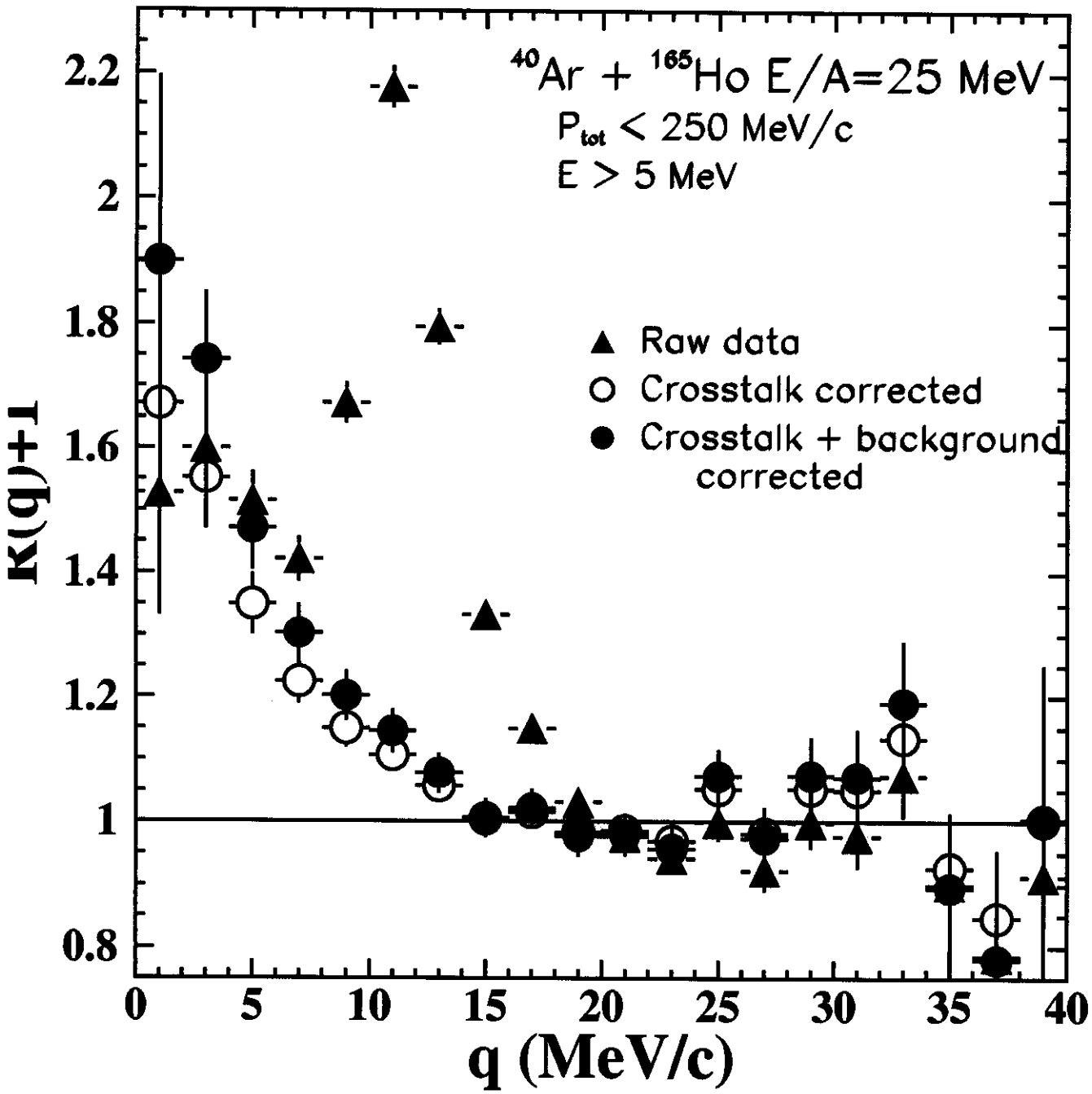
^{40}Ar + ^{165}Ho E/A=25 MeV
P_{tot} < 250 MeV/c
E > 5 MeV
Raw data
Crosstalk corrected
Crosstalk + background corrected
K(q)+1
q (MeV/c)
2.2
2
1.8
1.6
1.4
1.2
1
0.8
0
5
10
15
20
25
30
35
40

Figure 2

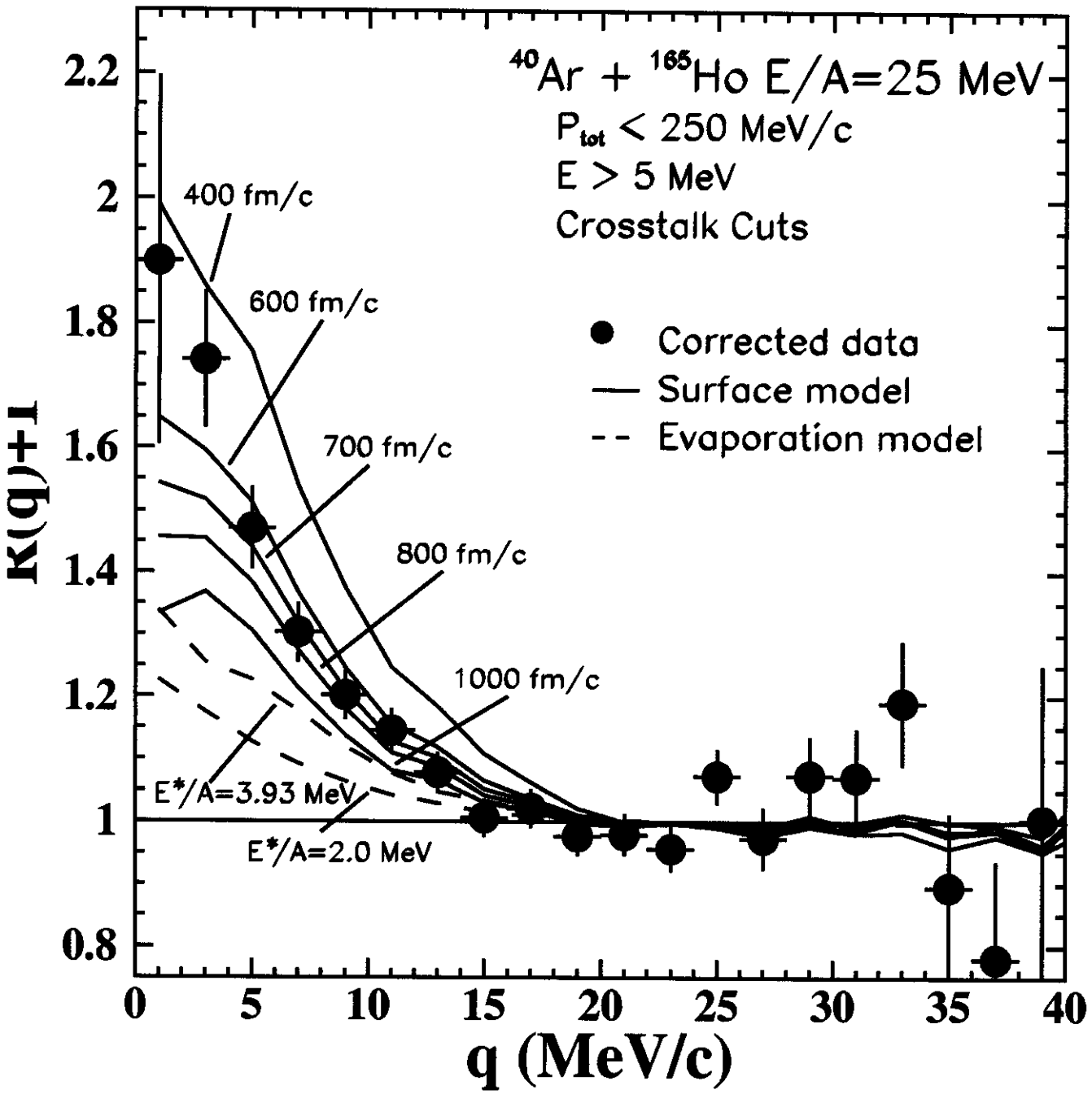
^{40}Ar + ^{165}Ho E/A=25 MeV
P_{tot} < 250 MeV/c
E > 5 MeV
Crosstalk Cuts
Corrected data
Surface model
Evaporation model
400 fm/c
600 fm/c
700 fm/c
800 fm/c
1000 fm/c
E*/A=3.93 MeV
E*/A=2.0 MeV
R(q)+1
q (MeV/c)
2.2
2
1.8
1.6
1.4
1.2
1
0.8
0
5
10
15
20
25
30
35
40

Figure 3

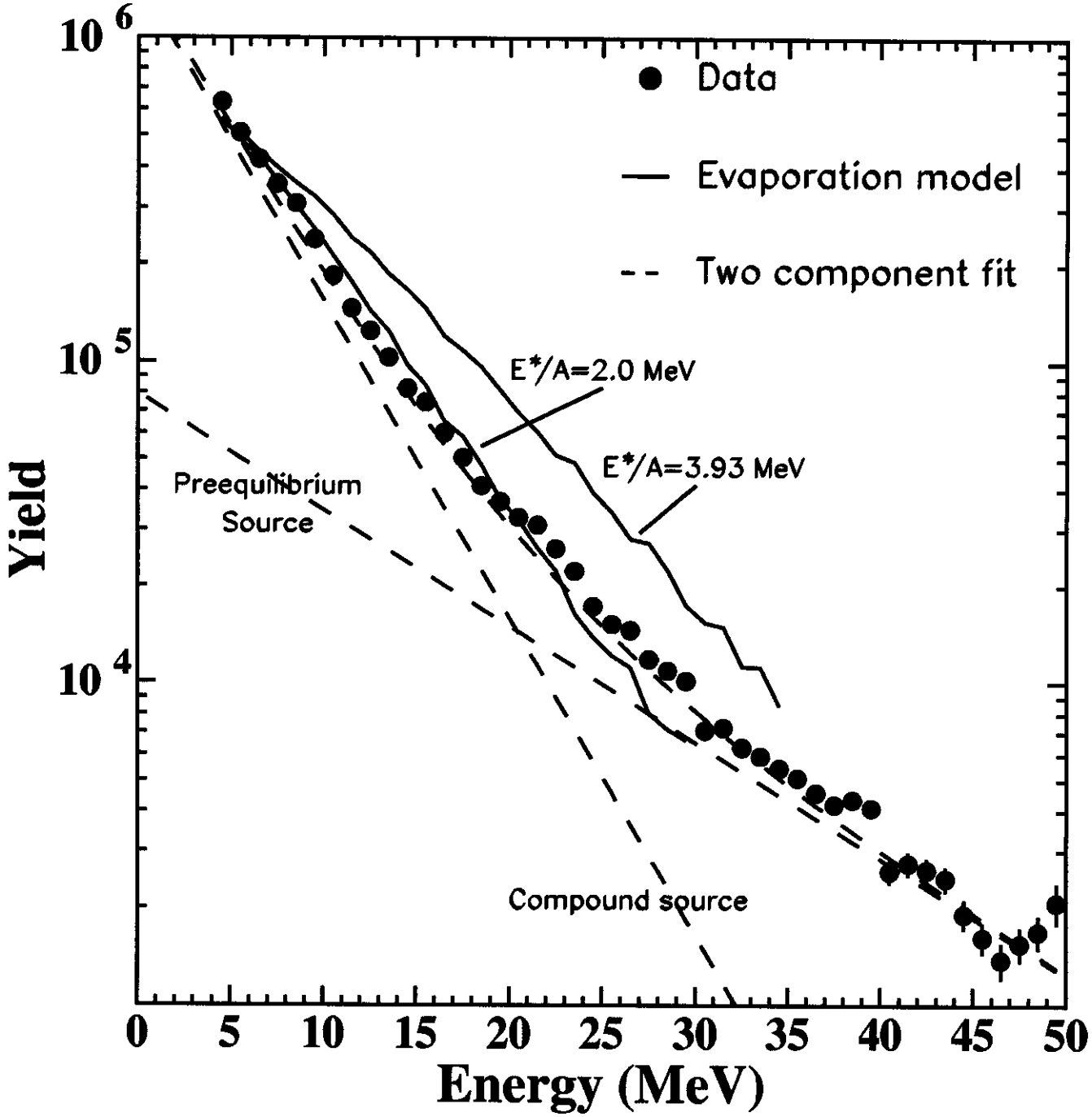
Data
Evaporation model
Two component fit
E*/A=2.0 MeV
E*/A=3.93 MeV
Preequilibrium Source
Compound source
Yield
Energy (MeV)
10 6
10 5
10 4
0
5
10
15
20
25
30
35
40
45
50

Figure 4

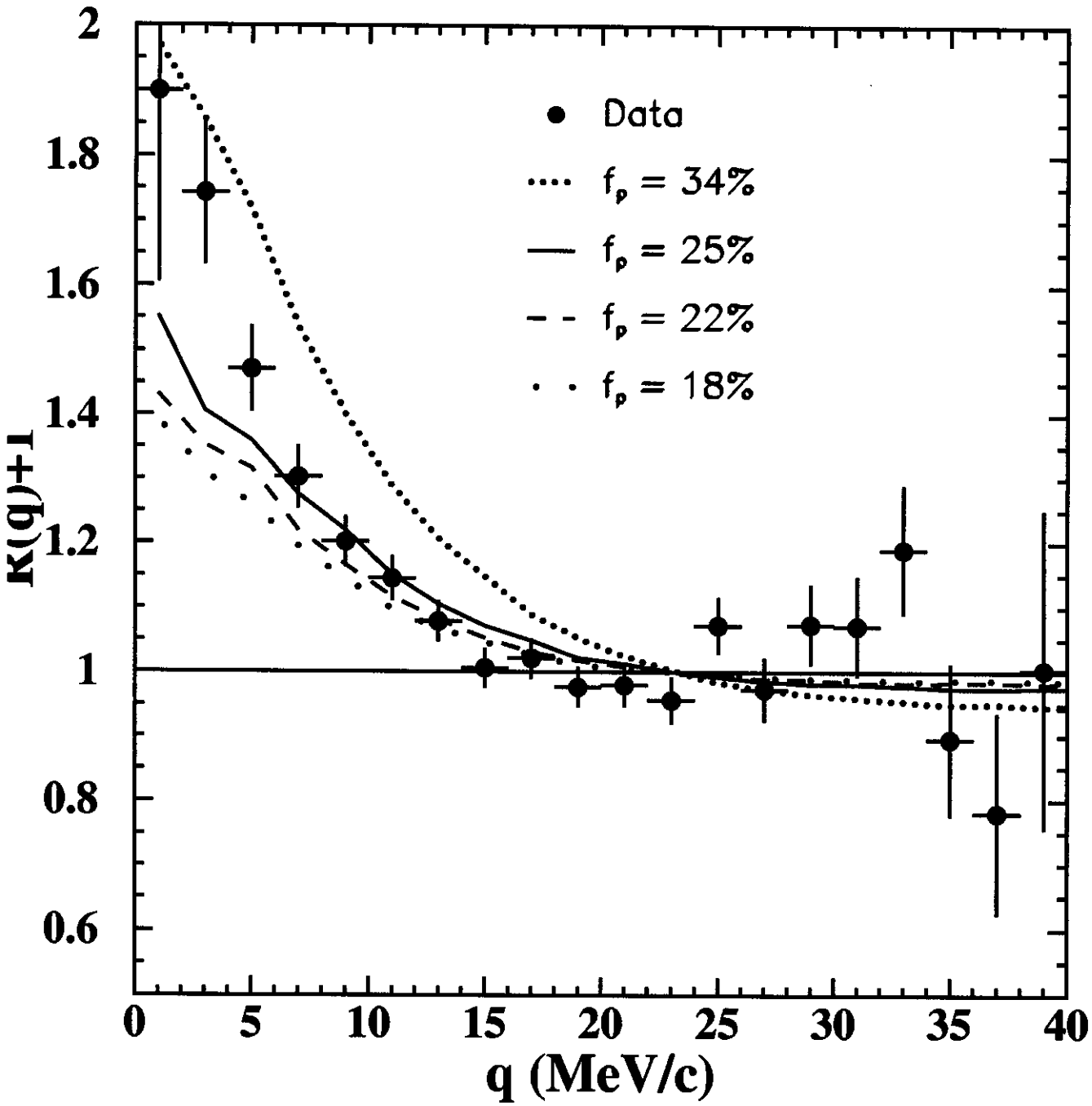
Data
f_p = 34%
f_p = 25%
f_p = 22%
f_p = 18%
K(q)+1
q (MeV/c)
2
1.8
1.6
1.4
1.2
1
0.8
0.6
0
5
10
15
20
25
30
35
40

Figure 5

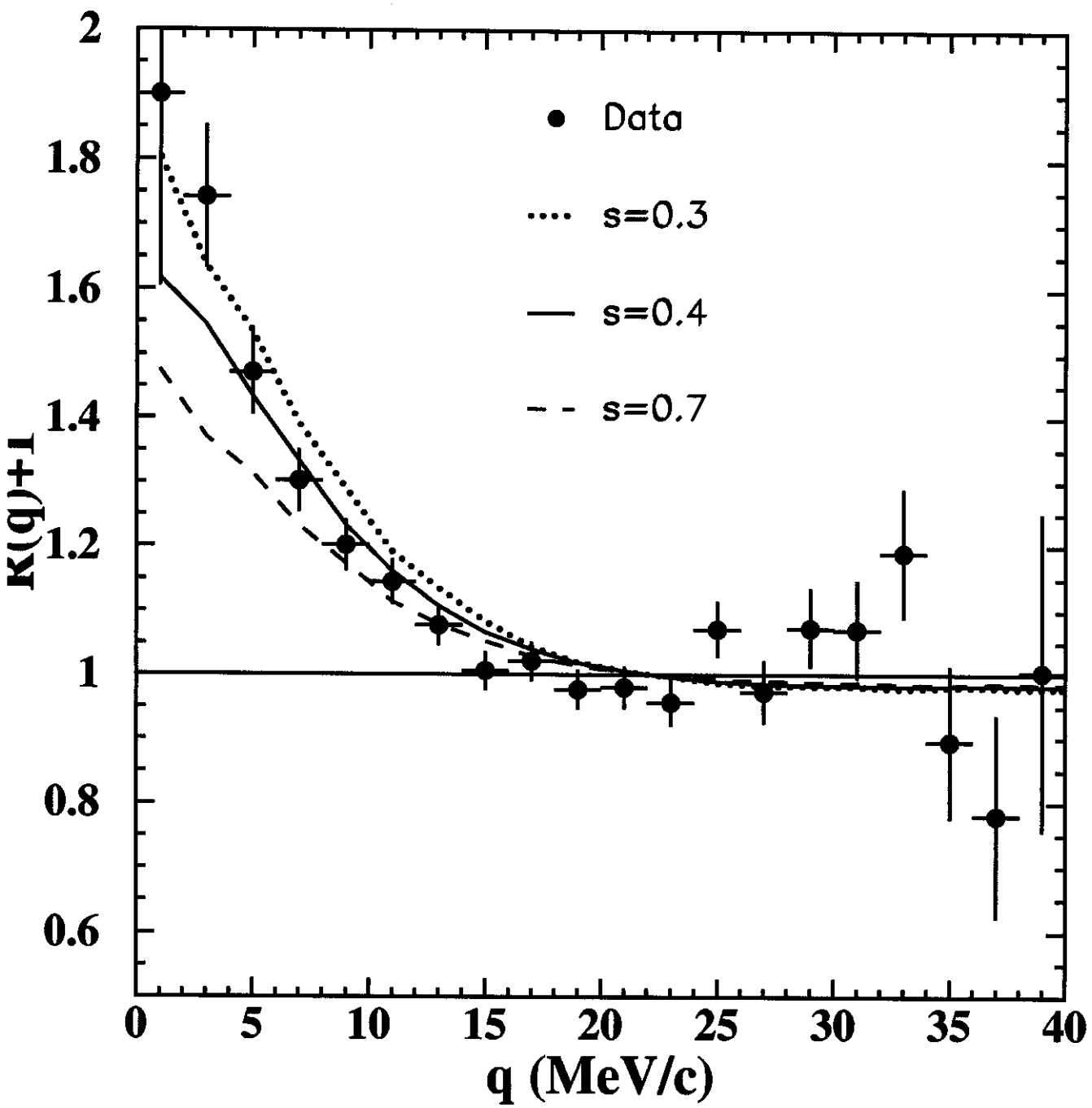
Data
s=0.3
s=0.4
s=0.7
K(q)+1
q (MeV/c)
2
1.8
1.6
1.4
1.2
1
0.8
0.6
0
5
10
15
20
25
30
35
40